Glass transition and positional ordering of hydrogen in bulk and nanocrystalline palladium

Hiroshi Akiba,[1,2] Hirokazu Kobayashi,[3,2] Hiroshi Kitagawa,[3,2] Maiko Kofu,[1,2] and Osamu Yamamuro[1,2,*]

[1]*Institute for Solid State Physics, University of Tokyo, Kashiwa, Chiba 277-8581, Japan*

[2]*Core Research for Evolutional Science and Technology (CREST), Japan Science and Technology Agency (JST), Chiyoda-ku, Tokyo 102-0076, Japan*

[3]*Graduate School of Science, Kyoto University, Sakyo-ku, Kyoto 606-8502, Japan*

(Received 22 January 2015; revised manuscript received 22 May 2015; published 21 August 2015)

Palladium hydride PdH_x ($0 < x < 1$), which may be the most well known metal hydride, still has some unexplained phenomena. In order to elucidate the origin of the "50 K anomaly," we have measured the heat capacity of the β phase of PdH_x ($x = 0.638$, 0.725, 0.782, 0.829) and $PdD_{0.641}$ by means of a custom-built adiabatic calorimeter. A steplike anomaly in heat capacity appeared at a temperature depending on x between 50 and 75 K. An exothermic effect followed by an endothermic one, implying an enthalpy relaxation to the equilibrium state, took place around the anomaly. This anomaly is attributed to not a phase transition as has been believed so far, but a glass transition corresponding to the freezing of the jump motion of hydrogen atoms in a short-range ordered state. If the hydrogen motion is not frozen, the completely ordered state could be realized at a hypothetical transition which appears below the glass transition temperature. Interestingly, the glass transition disappeared in PdH_x ($x = 0.553$, 0.629) and $PdD_{0.372}$ particles with a diameter of ca. 8 nm. This could be due to a quantum tunneling effect which is caused by surface and/or distortion effect of nanoparticles.

DOI: 10.1103/PhysRevB.92.064202 PACS number(s): 64.70.P−, 65.40.Ba, 66.30.Fq, 67.63.Gh

I. INTRODUCTION

Palladium hydride (PdH_x,$0 < x < 1$), which may be the most well known metal hydride, has attracted much attention due to its many exotic phenomena at low temperature; e.g., the 50 K anomaly [1], quantum diffusion of hydrogen [2], superconductivity at higher hydrogen concentration [3], etc. It has been noticed also in industry as a high-performance hydrogen storage material, and for catalysts, sensors, etc.

On absorption of hydrogen gas, a hydrogen molecule (H_2) dissociates into two hydrogen atoms (2H) and the H atoms occupy the interstitial sites of the Pd lattice. As shown in Fig. 1, PdH_x has two fcc phases depending on pressure p, temperature T, and H composition x; the α phase appears in a lower x region and the β phase in a higher x region. In the intermediate region (domelike area of Fig. 1), the α and β phases coexist. The plots in Fig. 1 show the absorption isotherms [4] at different temperatures (also called pressure-composition isotherm or PCT curve). The volume of the β phase is 11% larger than that of the α phase [5]. In the β phase, the hydrogen atoms occupy the octahedral sites in the Pd lattice as shown in Fig. 1.

The 50 K anomaly is one of the unsolved interesting problems in the PdH_x system. An anomaly is observed around 50 K in various physical quantities, e.g., heat capacity [1], electric resistivity [6], internal friction [7], and thermal relaxation [8]. To investigate the structure including hydrogen atoms, several neutron diffraction studies have been performed on palladium deuteride (PdD_x) [9–15]. Ellis *et al.* [9] reported the neutron diffraction data of a $PdD_{0.76}$ single crystal, indicating the ordering of D atoms in $I4/m$ (Ni_4Mo-type) structure. Anderson *et al.* [10,11] found another ordered structure of $I4_1/amd$ symmetry for $PdD_{0.64}$. Blaschko *et al.* [12] presented a phase diagram with the two ordered structures depending on the composition of D atoms. Kennedy's group performed neutron powder diffraction experiments [13,14] on $PdD_{0.65}$ and $PdD_{0.78}$, and argued that the former has a $Pm\bar{3}n$ structure with cell doubling and the latter has the $I4/m$ structure proposed by Ellis *et al.* It is of interest that thermal relaxation [8] was observed around 50 K and the intensity of the neutron diffraction peaks depended on time during the annealing around 50 K [15]. In spite of these previous works, there are still important unanswered problems; e.g., what is behind the complicated phase boundary violating the Gibbs' phase rule, the relation between the D atom ordering and the relaxation phenomena, and the isotope effect (H or D) on the above ordering process.

The physical and chemical properties of nanometer sized materials are of interest because they are often different from bulk properties [16,17]. Also for the nanoparticles of palladium hydrides there are drastic changes of the H_2 pressure-composition phase diagram [18,19], vibrational density of states [20,21], structures [22,23], etc. One interesting report related to the dynamics of H atoms is a quasielastic neutron scattering work by Janßen *et al.* [24], although the size of the nanoparticles was not defined. They found that nanoparticles of palladium have two relaxations: one is essentially the same relaxation as in the bulk sample and the other is 10^2 to 10^4 times faster than the relaxation in bulk. This effect can alter the 50 K anomaly drastically if it is related to a relaxation phenomenon.

Based on the information described above, we have studied the thermodynamic properties of bulk PdH_x ($x = 0.638$, 0.725, 0.782, 0.829), bulk $PdD_{0.641}$, nanoparticles of PdH_x ($x = 0.553$, 0.629) and nanoparticles of $PdD_{0.372}$ by means of adiabatic calorimetry which is suitable for investigating nonequilibrium phenomenon such as glass transitions and irreversible phase transition through a spontaneous exothermic or endothermic effect.

*yamamuro@issp.u-tokyo.ac.jp

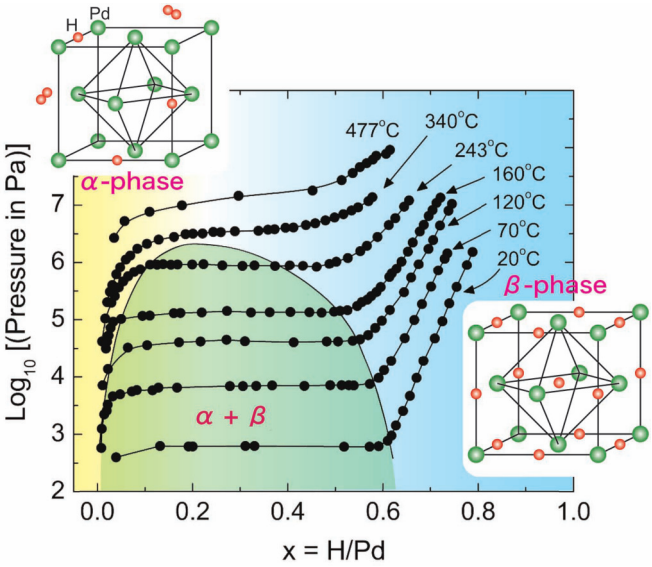

FIG. 1. (Color online) H_2 pressure-composition (p-x) phase diagram of the Pd-H system [4] and schematic structure of the α and β phases.

II. EXPERIMENT

The heat capacity measurement was carried out using a custom-built adiabatic calorimeter [25]. The adiabatic calorimetry consists of alternating sample heating and equilibration periods. The thermal equilibrium of sample is confirmed by observing the temperature drift (precision within ± 0.1 mK) during equilibration periods. When the equilibrium is established, the temperature drift rate becomes zero under adiabatic conditions. In nonequilibrium conditions, a spontaneous exothermic or endothermic drift due to the enthalpy relaxation is observed. In addition, adiabatic calorimetry is the most accurate method of determining the absolute value of heat capacity. The accuracy of the heat capacity measurement was better than 0.1% above 30 K. For the present experiment, we have developed a gas handling system and a small sample cell (inner volume 1.06 cm^3) with a transfer tube for *in situ* introduction of hydrogen gas into the sample cell.

The bulk Pd powder sample (526.7 mg), which was purchased from STREM CHEMICALS, was loaded into the sample cell and sealed with an indium gasket. The sample was annealed under vacuum above 80 °C for 3 hours to remove the water and air adsorbed on the Pd surface. Four PdH_x samples with different hydrogen composition were prepared by reacting Pd with H_2 gas at different temperatures and pressures. After two hours from the introduction of H_2 gas into the sample cell, the samples reached equilibrium under the following temperatures and H_2 pressures: (339 K, 18.37 kPa), (319 K, 97.83 kPa), (280 K, 100.19 kPa), (210 K, 100.03 kPa). From these results and the PCT curve in Fig. 1, the compositions of the obtained samples are estimated to be $x = 0.638, 0.725, 0.782, 0.829$, respectively. Since the volumes of the gas handling system and the sample cell were known, the amount of hydrogen absorbed in Pd was determined also from the H_2 pressure change in the sample preparation. These values were consistent with the x values determined from the PCT curve.

The preparation of the deuterated sample PdD_x was performed under D_2 gas atmosphere at 310 K and 0.1 MPa. The D_2 gas (D ratio > 99.9%) was purchased from TOMOE SHOKAI Co. Ltd. The absorption/desorption cycle of D_2 gas was repeated five times to achieve complete H/D substitution. The D composition x was determined to be 0.641 from the PCT curve [26] as in PdH_x.

Nanoparticles of Pd were obtained by the method described in the Supplemental Material [27] and a previous paper [28]. The obtained nanoparticles have a well-defined shape of an edge-cut octahedron and small size distribution as shown by transmission electron microscope (TEM) observation (see supplement, Fig. S1). The diameter of the nanoparticles was (8.0 ± 0.9) nm. The nanoparticles are covered with a protection polymer polyvinylpyrrolidone (PVP). The mass of the sample including PVP was 834.8 mg. The ratio of Pd and PVP was determined by elemental analysis to be 74.5 : 25.5. The procedure for the absorption of H_2 and D_2 gases in Pd nanoparticles was almost the same as for the bulk sample, but it took long time (3 to 4 days) to obtain an equilibrium state. The compositions of the nanoparticle samples of PdH_x were determined to be 0.553 and 0.629 from the PCT curve [19]. That of PdD_x was determined to be 0.372 from the pressure change due to the D_2 gas absorption since the PCT curve of PdD_x has not been reported so far. In evaluating the heat capacity of Pd nanoparticles, the contribution from PVP was subtracted from the total heat capacity. The heat capacity of PVP was measured separately as shown in the Supplemental Material (see Fig. S2).

III. RESULTS AND DISCUSSION

A. Heat capacity of PdH_x

Figure 2 shows the heat capacities of $PdH_{0.725}$ (red filled circles) and pure Pd (black open circles). For $PdH_{0.725}$, a heat capacity anomaly appeared around 55 K as expected from the previous work [1]. The heat capacity of $PdH_{0.725}$ is larger than that of Pd in the entire temperature region. We have fitted the

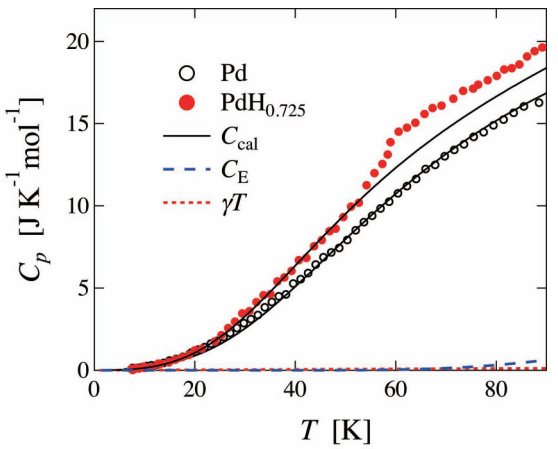

FIG. 2. (Color online) Heat capacities of $PdH_{0.725}$ and pure Pd. The black solid curves represent the results of the fittings to Eq. (1). The blue dashed and red dotted curves show the Einstein and electronic heat capacities, respectively.

data at temperatures lower than 55 K to the functions

$$C_{\rm cal} = C_{\rm D} + C_{\rm E} + \gamma T, \tag{1}$$

$$C_{\rm D} = 9R\left(\frac{T}{\theta_{\rm D}}\right)^3 \int_0^{\theta_{\rm D}/T} \frac{x^4 e^x dx}{(e^x-1)^2}, \tag{2}$$

$$C_{\rm E} = 3R\left(\frac{\theta_{\rm E}}{T}\right)^2 \frac{e^{\theta_{\rm E}/T}}{(e^{\theta_{\rm E}/T}-1)^2}, \tag{3}$$

where $C_{\rm D}$ and $C_{\rm E}$ correspond to the heat capacities due to the acoustic and optical vibrations, respectively and γT represents the electronic heat capacity. The parameters $\theta_{\rm D}$ and $\theta_{\rm E}$ are the Debye and Einstein temperatures, respectively. R is the gas constant. In the fitting, $\theta_{\rm E}$ was fixed to 661 K which was estimated from the peak energy (57 meV) of the optical vibration in an inelastic neutron scattering experiment [29]. The coefficient γ of the electronic heat capacity was also determined not by the fitting but by the interpolation for the previous heat capacity data at very low temperatures [30]. The black solid curves, which are the results of the fittings to Eq. (1), reproduce well the experimental data. As shown in Fig. 2, the Einstein and electronic heat capacities are not significant in this temperature range. The Debye temperature $\theta_{\rm D}$ for $PdH_{0.725}$ determined by the fitting is 246 K. This value is smaller than that of pure Pd ($\theta_{\rm D} = 281$ K), meaning that the Pd lattice is softened by accommodating H atoms. In the previous studies [1,31], the 50 K anomaly was treated as a C_p peak. From the precise analysis shown here, however, it is clearly a steplike anomaly.

Figure 3 shows the heat capacities of PdH_x ($x = 0.638$, 0.725, 0.782, 0.829). The anomaly gradually shifts to the higher temperature side with increasing x. This is in accordance with the previous work by Araki *et al.* [31]. At temperatures lower than the anomaly, the experimental data are reproduced well by Eq. (1) as shown by the solid curves in Fig. 3. The Debye temperature $\theta_{\rm D}$ determined by the fittings is almost independent of x in the β phase (see Table I).

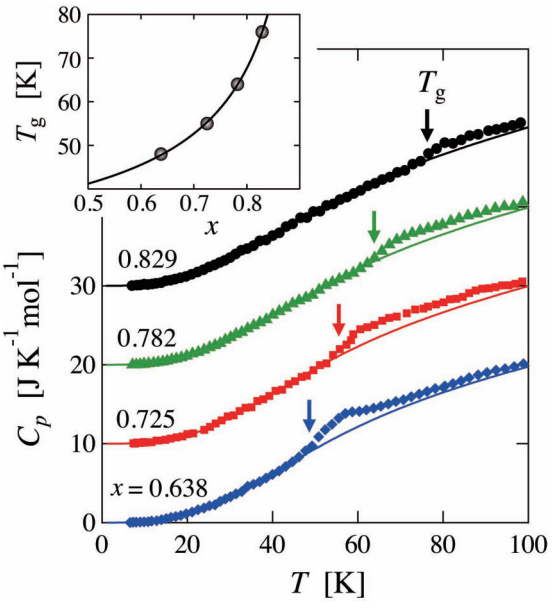

FIG. 3. (Color online) Heat capacity curves of PdH_x ($x = 0.638$, 0.725, 0.782, 0.829). Each curve is shifted upward by 10 J K^{-1}mol^{-1} for the sake of clarity. The arrows represent the glass transition temperatures $T_{\rm g}$ determined by the method described in the text. The inset shows the x dependence of $T_{\rm g}$. The curves shown in the C_p and $T_{\rm g}$ figures represent the results of the fittings to Eqs. (1) and (9), respectively. See text for details.

TABLE I. Parameters reproducing the experimental heat capacities and glass transition temperatures for bulk PdH_x and PdD_x.

	γ[a] (mJ K^{-2}mol^{-1})	$\theta_{\rm D}$ (K)	$\theta_{\rm E}$[b] (K)	$T_{\rm g}$ (K)
Pd	9.41	281.3 ± 0.7		
$PdH_{0.638}$	1.93	248.7 ± 0.6	661	48
$PdH_{0.725}$	1.38	245.9 ± 0.6	661	55
$PdH_{0.782}$	1.39	248.7 ± 0.6	661	64
$PdH_{0.829}$	1.46	247.0 ± 0.8	661	76
$PdD_{0.641}$	1.93	249.0 ± 0.3	484	51

[a]From heat capacity experiment at very low temperatures [30].
[b]From inelastic neutron scattering experiment [29,40].

B. Enthalpy relaxation and glass transition

We have also found an exothermic/endothermic phenomenon around the 50 K anomaly. Figure 4(a) shows the relaxation rate of configurational enthalpy ($-d\Delta H_{\rm c}/dt$) during the C_p measurement of $PdH_{0.782}$. This value was determined from the following equation:

$$-\frac{d\Delta H_{\rm c}}{dt} = \frac{dT}{dt} C(\text{total}) \tag{4}$$

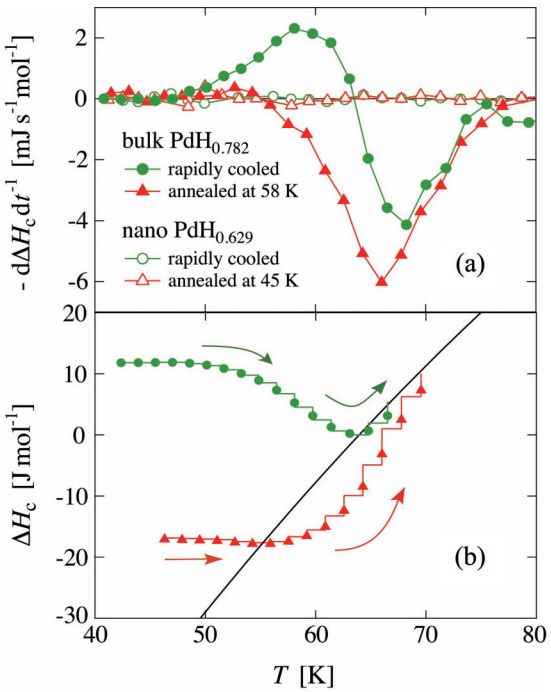

FIG. 4. (Color online) (a) Temperature dependence of the relaxation rate of configurational enthalpy for bulk $PdH_{0.782}$ (closed symbols) and nanoparticles of $PdH_{0.629}$ (open symbols). (b) Configurational enthalpy path during the heat capacity measurement of $PdH_{0.782}$.

where C(total) is the total heat capacity including the sample cell and dT/dt is the spontaneous temperature drift rate. The temperature drift rate was observed 5 min after each energy input. If there is no thermal anomaly in the sample, the thermal equilibrium of the sample cell is established within 5 min and the relaxation rate should be zero. For a sample cooled rapidly at a rate of 15 K/min, an exothermic, followed by an endothermic, enthalpy relaxation appeared in the temperature range 50–75 K as shown by the green filled circles in Fig. 4(a). The temperature at which the drift rate changes from positive to negative almost agrees with the onset temperature of the steplike C_p anomaly. For a sample annealed at 58 K for 5 hours, only an endothermic enthalpy relaxation appeared starting from the annealing temperature as shown by the red filled triangles in Fig. 4(a). This type of enthalpy relaxation, which accompanies the steplike C_p anomaly and depends on the thermal history of the sample, is one of the characteristic features of a glass transition [32]. The glass transition temperatures T_g was determined by taking the temperature at which the enthalpy relaxation rate of the rapidly cooled sample changes sign, as is usually done to determine T_g in the adiabatic calorimetry. The T_g's thus determined are tabulated in Table I and plotted as a function of x in the inset of Fig. 3.

Figure 4(b) shows the diagram of the configurational enthalpy ΔH_c related to the glass transition. The steplike line represents the enthalpy path during the actual heat capacity measurement. The horizonatal segment represents the temperature increase caused by supplying energy and the vertical one the enthalpy relaxed. The arrows represent the directions in which the heat capacity measurements were carried out. The filled symbols indicate the values of ΔH_c at the time when the relaxation rate in Fig. 4(a) was observed. The black curve gives the hypothetical equilibrium enthalpy derived by integrating the excess heat capacity above T_g [difference between the experimental data and the calculated curve C_{cal} in Eq. (1)]. The zero of ΔH_c was taken arbitrarily at $T_g = 64$ K.

In the rapidly cooled sample [green curve in Fig. 4(b)], the glassy state below T_g has an excess configurational enthalpy with respect to the equilibrium state. In the vicinity of T_g where the enthalpy relaxation time becomes comparable to the time scale of the heat capacity measurement (10^3 s), the enthalpy relaxation to the equilibrium state is observed as spontaneous exothermic processes. In the annealed sample [red curve in Fig. 4(b)], the endothermic enthalpy relaxation from the state with a deficient enthalpy to the equilibrium state is observed around T_g. Thus, we conclude that the 50 K anomaly is attributed to not a phase transition, as has been believed so far, but a glass transition corresponding to the freezing of the configurational motion of H atoms in Pd lattice. This is quite interesting in the sense that a glass transition, which is originally a phenomenon in liquid or polymer systems, occurs in a metal hydride.

Figure 5 shows the relaxation of configurational enthalpy observed during the annealing processes for the samples with $x = 0.725$ and 0.638. The annealing was performed at 50 and 44 K, respectively. The data were fitted to the function

$$\Delta H_c(T,t) = \Delta H_c(T,0)\exp\left(-\frac{t}{\tau}\right), \quad (5)$$

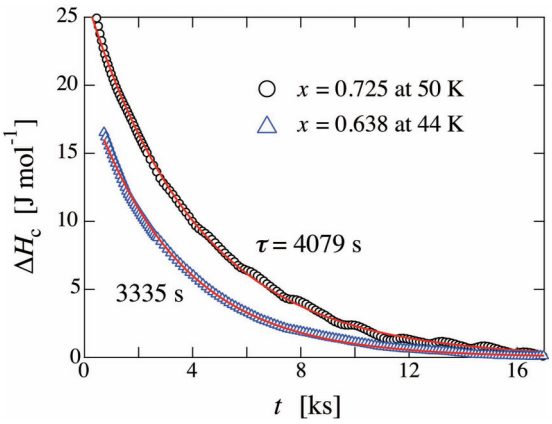

FIG. 5. (Color online) Enthalpy relaxations during annealing processes of $PdH_{0.725}$ and $PdH_{0.638}$. The red curves are the results of the fittings to Eq. (5). See text for details.

where τ is the relaxation time and $\Delta H_c(T,0)$ is the total amount of the relaxation. The fitting was carried out regarding τ and $\Delta H_c(T,0)$ as adjustable parameters. The result of the fitting was satisfactory as shown in Fig. 5. The determined relaxation times for $x = 0.725$ and 0.638 are 4079 and 3335 s, respectively.

Figure 6 presents the Arrhenius plot of the relaxation times τ of hydrogen jump motion for PdH_x ($0.6 < x < 0.7$) estimated from the various methods: quasielastic neutron scattering (QENS) [33,34], nuclear magnetic resonance (NMR) [35], internal friction [7], and thermal relaxation [8]. All of the data roughly fall on a single universal curve in a wide temperature range, indicating a common relaxation process of H atoms in Pd. The neutron scattering studies revealed that the relaxation is due to hydrogen jumps among the octahedral sites. The present τ's from the enthalpy relaxations, which are plotted by the filled circles, also coincide with the universal curve. This indicates that the origin of glass transition, corresponding to the enthalpy relaxation in Fig. 5,

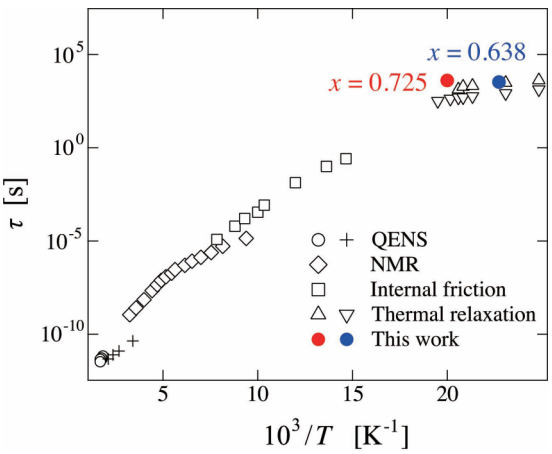

FIG. 6. (Color online) Relaxation times of the hydrogen motion in PdH_x ($0.6 < x < 0.7$) obtained from the various methods given in the legend. The results from the enthalpy relaxation are also plotted (red and blue filled circles).

is the freezing of the H atoms positionally disordered among the octahedral sites.

It is noteworthy that the Arrhenius plot is convex upward and has a small gradient at low temperature. This is opposite to the temperature dependence (convex downward) in supercooled water [36,37] and many of glass-forming liquids [38,39], both of which also have critical points or some related singularities on the low-temperature side of the glass transition. The unusual temperature dependence in palladium hydrides may be due to some quantum effect as suggested by Cornell and Seymour in their NMR paper [35]. The transfer of H atoms through a tunneling process, which has no temperature dependence in the ideal case, may become dominant at low temperature.

The inset of Fig. 3 demonstrates the x dependence of the glass transition temperature T_g. The T_g increases not linearly to x but more steeply at higher x. We proposed a simple model to explain this x dependence of T_g.

First, we assume that the temperature dependence of the relaxation time follows the Arrhenius relation,

$$\tau(T) = \frac{\tau_0}{p} \exp\left(\frac{\Delta E}{RT}\right), \tag{6}$$

where ΔE is the activation energy of the relaxation process, R is the gas constant, τ_0 is the relaxation time at the high-temperature limit, usually corresponding to the vibrational frequency of the H atom, and p is the jump probability depending on the local structure. We suppose that the jumps of H atoms occur only to the neighboring vacant (octahedral) sites. Then, the jump probability p is proportional to the number of vacant sites $1 - x$:

$$p = c\,(1 - x). \tag{7}$$

The $\tau(T)$ reaches 10^3 s around T_g:

$$\tau(T_g) = 10^3 \text{ s}. \tag{8}$$

From Eqs. (6)–(8), we derived the following equation:

$$T_g = \frac{\Delta E}{R\left[\ln(1 - x) + \ln\left(10^3 \text{ s} \times \frac{c}{\tau_0}\right)\right]}. \tag{9}$$

The observed T_g was fitted well to Eq. (9) using the fitting parameters ΔE and c/τ_0. The result of the fit is shown by the solid curve in the inset of Fig. 3. The ΔE and c/τ_0 were estimated to be 0.8 kJ mol^{-1} and 0.02 s^{-1}, respectively. It was revealed that the number of vacant sites governs the glass transition temperature in the Pd-H system. It is noteworthy that both values of ΔE and c/τ_0 are quite small, corresponding to the nearly flat curve with a large intercept (τ_0/p) in the low-temperature region of the Arrhenius plot (Fig. 6).

C. Heat capacity of $PdD_{0.641}$

Figure 7 shows the heat capacities of $PdD_{0.641}$. A heat capacity anomaly due to a glass transition appeared at around 55 K as observed in $PdH_{0.638}$ (see Fig. 3). This result indicates that the isotope effect on the 50 K anomaly is small. We have fitted the data at temperatures lower than 55 K to Eq. (1) with fixed parameters of an Einstein temperature θ_E (=484 K), obtained from the inelastic neutron scattering spectra [40] of

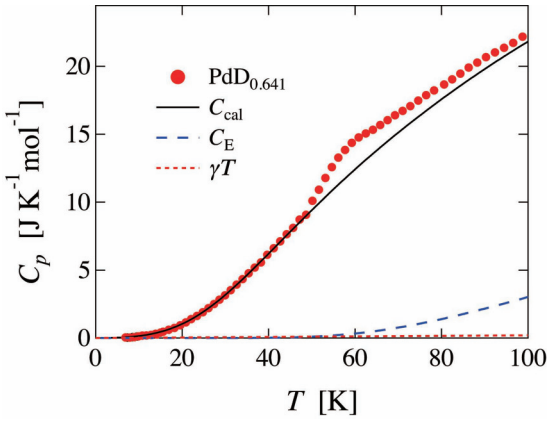

FIG. 7. (Color online) Heat capacities of $PdD_{0.641}$. The black curves represent the results of the fittings to Eq. (1). The blue dashed and red dotted curves show the heat capacities due to the optical vibration and conduction electrons, respectively.

PdD_x, and a coefficient γ (=1.93 mJ K^{-2}mol^{-1}), which is assumed to be the same as that of $PdH_{0.638}$ [30]. The Debye temperature θ_D was determined to be 249 K, which is almost the same as that of $PdH_{0.638}$ (248 K). Each component of heat capacity is shown in Fig. 7. It is remarkable that the Einstein heat capacity due to the optical vibration is important in $PdD_{0.641}$, in contrast to that of $PdH_{0.638}$, because of the mass effect ($m_D/m_H \approx 2$).

D. Positional ordering and hypothetical phase transition of D atoms

For the samples with the lowest x and T_g, i.e., for $PdH_{0.638}$ and $PdD_{0.641}$, the excess heat capacity above T_g was calculated by subtracting C_{cal} in Eq. (1) from the total heat capacity. They are plotted by the open symbols in Fig. 8. In order to investigate the origin of the excess heat capacities above T_g, we annealed the samples for 3 days at 50 K, where Bond *et al.* [15] annealed $PdD_{0.665}$ in their neutron diffraction experiment. They found that the intensity of the (1,1/2,0) superlattice peak increased with an increase of annealing time, indicating the gradual ordering of D atoms in the $I4_1/amd$ structure. As shown by closed symbols in Fig. 8, the excess heat capacities drastically increased by the annealing; they look like peaks rather than steps. Figure 9 presents the excess heat capacities divided by temperature (upper) of $PdD_{0.641}$ and the excess entropies (lower) calculated from the integration of the $\Delta C_p/T$ data. The data for both annealed and normally cooled samples are plotted. The blue dashed lines are theoretical curves for the two-dimensional Ising model with a hypothetical transition temperature T_c of 47.5 K; it should be noted that this curve does not claim the mechanism of the transition but is just to facilitate understanding. These plots strongly indicate that the excess heat capacity above T_g is a so-called high-temperature tail of the transition that is due to the short-range ordering of D atoms. The excess entropy due to the short-range ordering is 1.85 J K^{-1}mol^{-1}, which corresponds to 34% of the total transition entropy calculated by

$$\Delta_{mix} S = -R[x \ln x + (1 - x)\ln(1 - x)]. \tag{10}$$

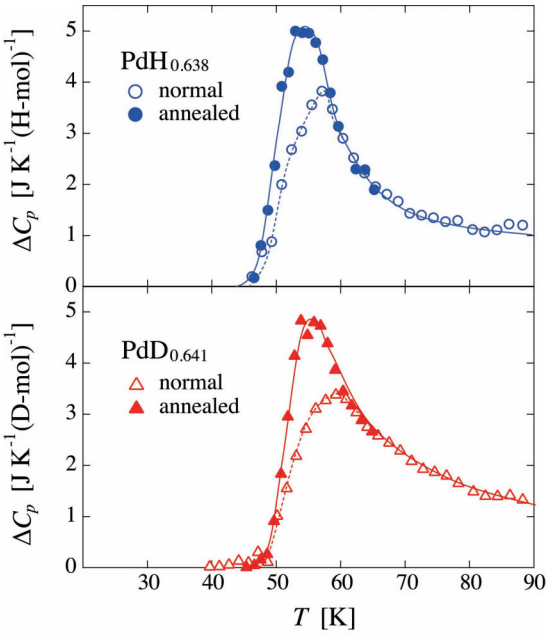

FIG. 8. (Color online) Excess heat capacities of $PdH_{0.638}$ (upper) and $PdD_{0.641}$ (lower) above T_g's. The data for normally cooled and annealed (50 K, 3 days) samples are plotted by open and closed symbols, respectively. See text for details.

Here, $\Delta_{mix}S$ is the mixing entropy and calculated to be 5.43 $J K^{-1} mol^{-1}$ for $x = 0.641$.

The entropy gained by the annealing was 2.07 $J K^{-1} mol^{-1}$, which corresponds to 38% of the total transition entropy. Thus,

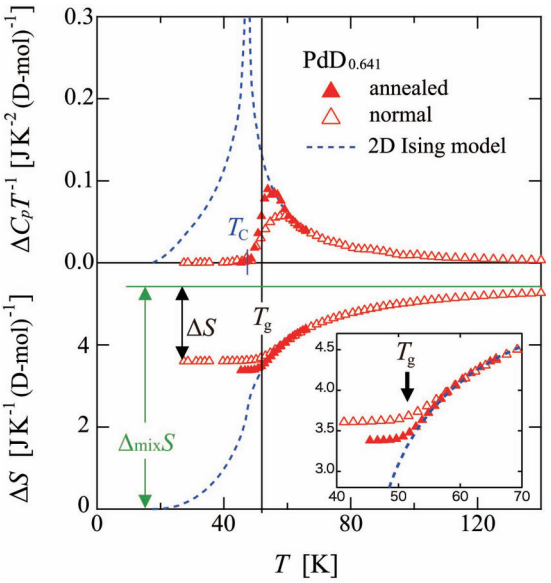

FIG. 9. (Color online) Excess heat capacities divided by temperature (upper) and the excess entropies (lower) of $PdD_{0.641}$. The data for normally cooled and annealed (50 K, 3 days) samples are plotted by open and closed symbols, respectively. The inset shows the ΔS around T_g in an enlarged scale. The blue dashed lines are theoretical curves for the two-dimensional Ising model with a hypothetical transition temperature T_c of 47.5 K. See text for details.

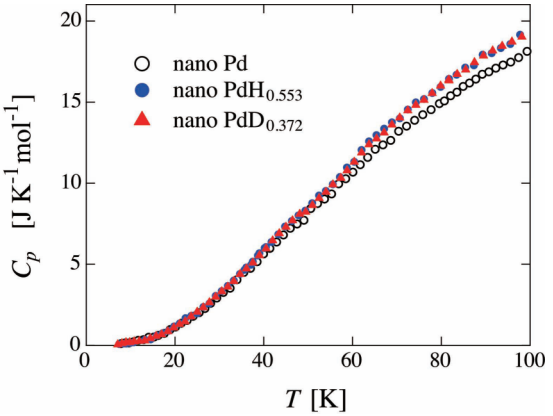

FIG. 10. (Color online) Heat capacities of nanoparticles of pure Pd, $PdH_{0.553}$, and $PdD_{0.372}$.

we have revealed that the 50 K anomaly of PdH_x and PdD_x is not due to the ordering transition but due to the freezing of the hydrogen atoms in a short-range ordered state. The superlattice peaks observed in the neutron scattering experiments are also not due to the completely ordered structure but are due to a short-range ordering of the hydrogen atoms. If the transition temperature was 5 K higher or the relaxation time was 1000 times shorter at around 50 K, the ordering transition would actually occur as in ordinary disordered systems.

The glass transitions of disordered crystals usually occur on the low-temperature side of their ordering transitions where the crystals are mostly ordered. There are many of such examples in molecular [41,42], ionic [43], hydrogen-bonded [44,45], and alloy [46] crystals. It is a rare case that T_g of palladium hydride is higher than its hypothetical T_c. The similar situations are found only in H_2O ice [47], carbon monoxide [48], and RbCN [49] to the best of our knowledge. In the case of H_2O ice, where a glass transition due to the freezing of the molecular reorientation occurs at 100 K [47], KOH doping accelerates the molecular reorientation and induces the actual ordering transition at 72 K [50–52].

E. Heat capacities of nanoparticles of PdH_x and PdD_x

Figure 10 shows the heat capacities of nanoparticles of Pd, $PdH_{0.553}$, and $PdD_{0.372}$. It is noteworthy that the heat capacities below 20 K are almost the same for the three samples, indicating that there is no effect of H_2 absorption on the lattice and electronic heat capacity.

Figure 11 shows the excess heat capacities of the bulk and nanoparticles of palladium hydrides. For the bulk samples, the excess heat capacity ΔC_p was calculated by subtracting C_{cal} in Eq. (1) from the total heat capacity (C_p in Fig. 3). On the other hand, in the nanoparticle samples, the heat capacities of nano-Pd before H_2 absorption were subtracted from the total heat capacity because the heat capacities of the hydrogenated and nonhydrogenated samples are almost the same below 20 K, as described above. The ΔC_p values per mole of H atoms are plotted in Fig. 11.

In the bulk samples, the jumps at T_g's are shown more clearly than in Figs. 2 and 3. The ΔC_p rises up at T_g and gradually decreases at higher temperatures. This shape of ΔC_p

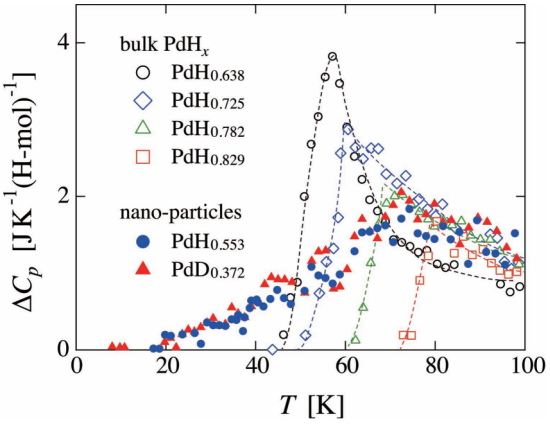

FIG. 11. (Color online) Excess heat capacities of bulk (open symbols) and nanoparticles (closed symbols) of PdH_x and PdD_x.

reflects the development of short-range ordering of H atoms as described above. In the nanoparticles, very interestingly, a step due to the glass transition disappeared. A temperature drift rate characteristic to glass transitions also disappeared as shown in Fig. 4(a). Thus, we can conclude that the glass transition disappeared in the nanoparticles of PdH_x. The ΔC_p of nano-PdH_x in Fig. 11 could be due to the gradual ordering process in the H atom positions.

Why did the glass transition disappear in nano-PdH_x? This may be related to the QENS work [24] mentioned in Sec. I. One reasonable explanation is that the H atom transfer occurs through a quantum tunneling process in a potential energy surface modified by surface and/or distortion effect of nanoparticles. It is possible that the tetrahedral sites, which are metastable sites in bulk Pd, are stabilized by the effect. The tunneling process could not be a pure tunneling between ground states but a sort of phonon assisted tunneling between excited states since there is temperature dependence of the relaxation times in the QENS experiments. This phenomenon may be associated also with the fact that H atoms are preferably located around the surface and subsurface in metal hydrides [53–55].

IV. CONCLUSION

We have revealed that the "50 K anomaly," which is the most long-standing problem in PdH, is not a phase transition as has been believed so far, but a glass transition due to the freezing of the jump motion of H atoms in the Pd lattice. It was found that the excess heat capacity above T_g is due to a short-range ordering of D atoms. If the hydrogen motion is not frozen, the completely ordered state could be realized at a hypothetical transition which appears below the glass transition temperature. The glass transition disappears in nanoparticles of PdH. This could be due to a quantum tunneling effect which is caused by surface and/or distortion effect of nanoparticles. To confirm the above conclusion on the nanoparticles, we are planning to undertake precise structure and QENS works using the same sample as in the C_p measurement.

ACKNOWLEDGMENTS

The authors thank Prof. S. Matsumura (Kyushu University) and the members of his laboratory for their works on the photographs via transmission electron microscope shown as Fig. S1 in the Supplemental Material [27].

[1] D. M. Nace and J. G. Aston, J. Am. Chem. Soc. **79**, 3627 (1957).
[2] I. Svare, Physica B **141**, 271 (1986).
[3] T. Skoskiewicz, Phys. Status Solidi A **11**, K123 (1972).
[4] H. Frieske and E. Wicke, Ber. Bunsenges. Phys. Chem. **77**, 48 (1973).
[5] P. Abens and W. G. Burgers, Trans. Faraday Soc. **58**, 1989 (1962).
[6] T. Skoskiewicz and B. Baranowski, Phys. Status Solidi B **30**, K33 (1968).
[7] J. K. Jacobs, C. R. Brown, V. S. Pavlov, and F. D. Manchester, J. Phys. F **6**, 2219 (1976).
[8] J. K. Jacobs and F. D. Manchester, J. Phys. F **7**, 23 (1977).
[9] T. E. Ellis, C. B. Satterthwaite, M. H. Mueller, and T. O. Brun, Phys. Rev. Lett. **42**, 456 (1979).
[10] I. S. Anderson, C. J. Carlile, and D. K. Ross, J. Phys. C **11**, L381 (1978).
[11] I. S. Anderson, D. K. Ross, and C. J. Carlile, Phys. Lett. A **68**, 249 (1978).
[12] O. Blaschko, Phys. Rev. B **29**, 5187 (1984).
[13] S. J. Kennedy, E. Wu, E. H. Kisi, E. M. Gray, and B. J. Kennedy, J. Phys.: Condens. Matter **7**, L33 (1995).
[14] E. Wu, S. J. Kennedy, E. M. Gray, and E. H. Kisi, J. Phys.: Condens. Matter **8**, 2807 (1996).
[15] R. A. Bond, I. S. Anderson, B. S. Bowerman, C. J. Carlile, D. J. Picton, D. K. Ross, D. G. Witchell, and J. K. Kjems, NATO Conf. Ser. **6**, 189 (1983).
[16] G. Schmid, *Clusters and Colloids* (VCH, Weinheim, 1994).
[17] S. Sugano and H. Koizumi, *Microcluster Physics* (Springer, Berlin, 1998).
[18] C. Sachs, A. Pundt, R. Kirchheim, M. Winter, M. T. Reetz, and D. Fritsch, Phys. Rev. B **64**, 075408 (2001).
[19] M. Yamauchi, R. Ikeda, H. Kitagawa, and M. Takata, J. Phys. Chem. C **112**, 3294 (2008).
[20] U. Stuhr, H. Wipf, T. J. Udvic, J. Weißmüller, and H. Gleiter, J. Phys.: Condens. Matter **7**, 219 (1995).
[21] U. Stuhr, H. Wipf, K. H. Andersen, and H. Hahn, Physica B **276-278**, 882 (2000).
[22] M. Suleiman, N. M. Jisrawi, O. Dankert, M. T. Reetz, C. Bahtz, R. Kirchheim, and A. Pundt, J. Alloys Compd. **356-357**, 644 (2003).
[23] J. A. Eastman, L. J. Thompson, and B. J. Kestel, Phys. Rev. B **48**, 84 (1993).
[24] S. Janßen, H. Natter, R. Hempelmann, T. Striffler, U. Stuhr, H. Wipf, H. Hahn, and J. C. Cook, NanoStruct. Mater. **9**, 579 (1997).
[25] O. Yamamuro, M. Oguni, T. Matsuo, and H. Suga, Bull. Chem. Soc. Jpn. **60**, 1269 (1987).
[26] R. Lasser and K. H. Klatt, Phys. Rev. B **28**, 748 (1983).
[27] See Supplemental Material at http://link.aps.org/supplemental/10.1103/PhysRevB.92.064202 for the synthesis of Pd nanoparticles and the heat capacity of PVP.

[28] B. Lim, M. Jiang, P. H. C. Camargo, E. C. Cho, J. Tao, X. Lu, Y. Zhu, and Y. Xia, Science **324**, 1302 (2009).
[29] M. R. Chowdhury and D. K. Ross, Solid State Commun. **13**, 229 (1973).
[30] C. A. Mackliet and A. I. Schindler, Phys. Rev. **146**, 463 (1966).
[31] H. Araki, M. Nakamura, S. Harada, T. Obata, N. Mikhin, V. Syvokon, and M. Kubota, J. Low Temp. Phys. **134**, 1145 (2004).
[32] H. Suga, J. Phys.: Condens. Matter **15**, S775 (2003).
[33] G. Nelin and K. Skold, J. Phys. Chem. Solids **36**, 1175 (1975).
[34] M. M. Beg and D. K. Ross, J. Phys. C **3**, 2487 (1970).
[35] D. A. Cornell and E. F. W. Seymour, J. Less-Common Met. **39**, 43 (1975).
[36] L. Liu, S.-H. Chen, A. Faraone, C.-W. Yen, and C.-Y. Mou, Phys. Rev. Lett. **95**, 117802 (2005).
[37] K. Yoshida, T. Yamaguchi, S. Kittaka, M.-C. Bellissent-Funel, and P. J. Fouqet, J. Chem. Phys. **129**, 054702 (2008).
[38] C. A. Angell, J. Phys. Chem. Solids **49**, 863 (1988).
[39] C. A. Angell, J. Non-Cryst. Solids **131-133**, 13 (1991).
[40] J. M. Rowe, J. J. Rush, J. E. Schirber, and J. M. Mintz, Phys. Rev. Lett. **57**, 2955 (1986).
[41] T. Matsuo, H. Suga, W. I. F. David, R. M. Ibberson, P. Bernier, A. Zahab, C. Fabre, A. Rassat, and A. Dworkin, Solid State Commun. **83**, 711 (1992).
[42] O. Yamamuro, M. Hayashi, T. Matsuo, and P. Lunkenheimer, J. Chem. Phys. **119**, 4775 (2003).
[43] K. Moriya, T. Matsuo, and H. Suga, J. Phys. Chem. Solids **44**, 1103 (1983).
[44] M. Oguni, T. Matsuo, H. Suga, and S. Seki, Bull. Chem. Soc. Jpn. **50**, 825 (1977).
[45] T. Matsuo, M. Oguni, H. Suga, S. Seki, and J. F. Nagle, Bull. Chem. Soc. Jpn. **47**, 57 (1974).
[46] S. Wei, I. Gallino, R. Busch, and C. A. Angell, Nat. Phys. **7**, 178 (2011).
[47] O. Haida, T. Matsuo, H. Suga, and S. Seki, J. Chem. Thermodyn. **6**, 815 (1974).
[48] T. Atake, H. Suga, and H. Chihara, Chem. Lett. **5**, 567 (1976).
[49] T. Shimada, T. Matsuo, H. Suga, and F. Luty, J. Chem. Phys. **85**, 3530 (1986).
[50] Y. Tajima, T. Matsuo, and H. Suga, Nature (London) **299**, 810 (1982).
[51] C. M. B. Line and R. W. Whitworth, J. Chem. Phys. **104**, 10008 (1996).
[52] S. M. Jackson, V. M. Nield, R. W. Whitworth, M. Oguro, and C. C. Wilson, J. Phys. Chem. B **101**, 6142 (1997).
[53] J. M. Nicol, J. J. Rush, and R. D. Kelley, Phys. Rev. B **36**, 9315 (1987).
[54] M. Wilde and K. Fukutani, Phys. Rev. B **78**, 115411 (2008).
[55] M. Wilde, K. Fukutani, M. Naschitzki, and H. J. Freund, Phys. Rev. B **77**, 113412 (2008).